Available online at www.sciencedirect.com
ScienceDirect
Advances in Space Research 44 (2009) 1314–1320
ADVANCES IN SPACE RESEARCH (a COSPAR publication)
www.elsevier.com/locate/asr

Asymmetric precipitation in a coronal loop as explanation of a singular observed spectrum

G. Cristiani [a,*,1], C.G. Giménez de Castro [b], C.H. Mandrini [a,1], M.E. Machado [c], M.G. Rovira [a,1]

[a] Instituto de Astronomía y Física del Espacio, CONICET-UBA, CC 67, Suc. 28, 1428 Buenos Aires, Argentina
[b] Centro de Rádio Astronomia e Astrofísica Mackenzie, Escola de Engenharia, R. da Consolação 896, 01302-907 São Paulo, SP, Brazil
[c] Comisión Nacional de Actividades Espaciales, Av. Paseo Colón 751, 1063 Buenos Aires, Argentina

Received 30 December 2008; received in revised form 2 June 2009; accepted 16 June 2009

Abstract

Almost 10 years of solar submillimeter observations have shown new aspects of solar activity, such as the presence of rapid solar spikes associated with the launch of coronal mass ejections and an increasing submillimeter spectral component in flares. We analyse the singular microwave–submillimeter spectrum of an M class solar flare on 20 December, 2002. Flux density observations measured by Sun patrol telescopes and the Solar Submillimeter Telescope are used to build the radio spectrum, which is fitted using Ramaty's code. At submillimeter frequencies the spectrum shows a component different from the microwave classical burst. The fitting is achieved proposing two homogeneous sources of emission. This theoretical fitting is in agreement with differential precipitation through a magnetically asymmetric loop or set of loops. From a coronal magnetic field model we infer an asymmetric magnetic structure at the flare location. The model proposed to quantify the differential precipitation rates due to the asymmetry results in a total precipitation ratio $Q_2/Q_1 \approx 10^4$–10^5, where $Q_1(Q_2)$ represents the total precipitation in the loop foot with the high (low) magnetic field intensity. This ratio agrees with the electron total number ratio of the two sources proposed to fit the radio spectrum.

Keywords: Sun: flares; Sun: radio radiation

1. Introduction

Solar submillimeter observations in a routinely manner began in 1999 with the Solar Submillimeter Telescope (SST) installation (Kaufmann et al., 2000). Although the number of observed events is relatively small (lower than two dozen), generally these events present remarkable features. The most important discovery at submillimeter frequencies is probably the presence of an increasing spectral component above 200 GHz in some impulsive radio bursts (Kaufmann et al., 2004, 2007; Lüthi et al., 2004; da Silva et al., 2007), called the THz component. The events showing this component are of X class. Although the gyrosynchrotron emission of accelerated electrons is the most plausible mechanism in the microwave–submillimeter range during the impulsive phase of flares, it cannot explain the observed spectral shape in these events.

In this work, we extend the spectral analysis of a burst with two spectral components previously studied by Cristiani et al. (2008) (hereafter Paper I). These two components are: the classical microwave spectrum and a high frequency component with a peak in the submillimeter range, which occurred during an M6.8 class flare. Unlike THz bursts, this event presents a submillimeter component that does not increase with frequency. We propose as

* Corresponding author. Tel.: +54 11 4781 6755; fax: +54 11 4786 8114.
E-mail addresses: gcristiani@iafe.uba.ar, gcristiani@gmail.com (G. Cristiani).
[1] Member of the Carrera del Investigador Científico, CONICET, Argentina.

0273-1177/$36.00 © 2009 COSPAR. Published by Elsevier Ltd. All rights reserved.
doi:10.1016/j.asr.2009.06.012

origin of this peculiar spectrum an asymmetric electron precipitation in coronal loop feet. This asymmetric precipitation, at two coronal loop feet with different magnetic field intensity, can be understood as the combined gyrosynchrotron emission of two populations of accelerated electrons in two homogeneous sources (see Paper I).

This paper is organized as follows: in Section 2 we summarize the radio observations in the microwave–submillimeter range and show the spectral fitting obtained considering two homogeneous sources of gyrosynchrotron emission. An asymmetric-loop emission model is outlined in Section 3.1 and this theory is applied to the data in Section 3.2 using results from the coronal magnetic model already discussed in Paper I. Our main conclusions are presented in Section 4.

2. Summary of the observations and previous results

The radio burst analysed in this work occurred on 20 December 2002 around 13:15 UT in active region (AR) 10226. In soft X-rays the event was classified as M6.8 and as a subflare in $H\alpha$. In the microwave range two events are detected with approximately 2 min separation. Radio observations correspond to SST, USAF Radio Solar Telescope Network (RSTN), Bern patrol telescopes and the two-element nulling interferometer of the University of Bern. The coverage in frequency is from 1.415 to 405 GHz. In the first event the submillimeter telescope was performing calibration routines; then, we restrict our analysis to the second event where the spectrum presents the submillimeter component. At 212 GHz the burst is clearly visible, while at 50, 89.4, and 405 GHz the noise dominates the emission and only an upper bound can be determined. In $H\alpha$ we have images from the $H\alpha$ Solar Telescope for Argentina (HASTA). These images show kernels (Fig. 1) that brighten with different timing. Full disk magnetograms from the Michelson Doppler Imager (MDI) were used in the analysis of the event. These magnetograms were used as boundary condition for a coronal magnetic field extrapolation. Fig. 2 shows the field connectivity in the flare region. The presence of an asymmetric loop or set of loops can be inferred from the model. The $H\alpha$ kernels lie at the feet of these reconnected loops (see Fig. 5 in Paper I).

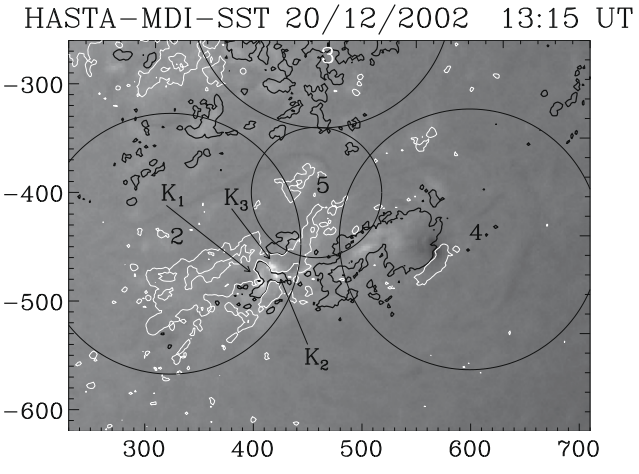

Fig. 1. An $H\alpha$ image at 13:15:43 UT showing the three kernels. MDI contours of ±100 G have been added (white/black colour corresponds to positive/negative values). Superimposed on the image, the circles represent the SST beams at the time of the burst. Beams 2, 3, and 4 (212 GHz) are the multibeam system. Beam 5 is the 405 GHz receiver. K_1, K_2 and K_3 indicate the position of the $H\alpha$ kernels. Both axes are measured in arcsec.

Fig. 3 shows the observed spectrum at the peak-burst time and the theoretical fitting. It is not possible to adjust the data with a single spectral curve of gyrosynchrotron emission. In the microwave range we consider a source and an electron beam with the parameters shown in Table 1 (called Source 2, in agreement with the theory developed in Section 3.1). To fit the submillimeter range we use a second source and electron beam, as indicated in the same table. The fitting in this frequency range is more difficult because we have only one point (212 GHz) and two upper bounds (89.4 and 405 GHz); nevertheless, we can restrict the space of solutions taking into account the extrapolated magnetic field intensities and reasonable electron beam density values. For a more exhaustive discussion about the physical parameters involved in the fitting see Paper I.

From Table 1, we observe that the second source (Source 1), responsible for the submillimeter spectral component, involves a total number of accelerated electrons approximately 5 orders of magnitude lower than the first one. Table 1 shows that, in order to fit the observations, the total number of emitting electrons is 5 orders smaller

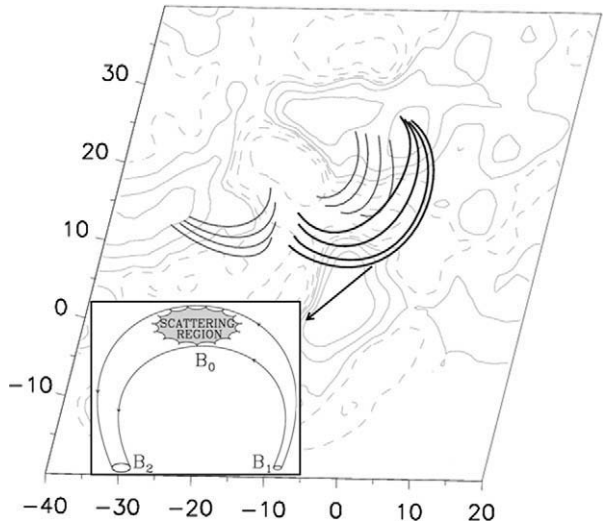

Fig. 2. Magnetic field model showing the field line connectivity in the vicinity of flare kernels in the observer's point of view. Thin continuous field lines represent the connectivities before magnetic reconnection has occurred, while thick continuous field lines are the ones after reconnection. The isocontours of the field are ±100, 500, 1000 G. Positive/negative isocontours are drawn with gray continuous/dashed thin lines. The axes are measured in Mm. The magnetic trap geometry is shown in the insert. In our example the magnetic field intensity at the loop feet verifies $B_1 > B_2$ with the same orientation as the asymmetric loop or set of loops in AR 10226.

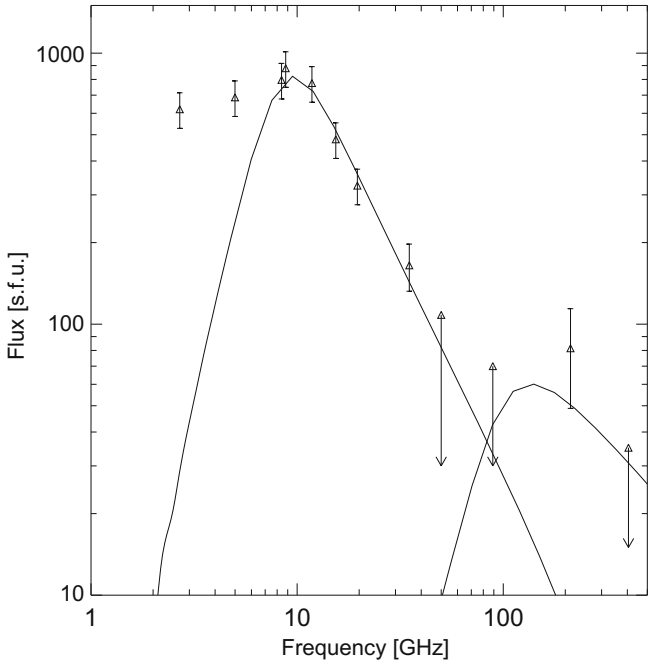

Fig. 3. Radio spectra at the burst peak time. The curves represent the obtained gyrosynchrotron solutions.

in Source 1 respect to Source 2. Eventually these electrons precipitate leading to a strikling precipitating ratio $Q_1/Q_2 \sim 10^{-5}$. This unusual ratio is what we explain below using a well accepted theory of asymmetric precipitation (Melrose and White, 1981).

3. Data analysis

3.1. Asymmetric precipitation model

The theory used to compute the precipitation rates has been developed by Melrose and White (1981) for asymmetric flux tubes. The main mechanism for trapped fast particle precipitation in a magnetic flux tube is the pitch-angle scattering. Three kinds of asymmetry are considered: the geometrical asymmetry due to the flux tube shape (loss cones of different sizes), the pitch-angle diffusion coefficient depending on the velocity, and an asymmetric particle injection into the flux tube. The model assumes a localized scattering region (at the top of the coronal loop, see insert in Fig. 2); then, the pitch-angle scattering can be approximately described by a local diffusion equation. For simplicity the steady state solutions are considered.

The loss cones are defined by

$$\alpha_1 = \arcsin\left(\sqrt{\frac{B_0}{B_1}}\right) \quad \alpha_2 = \arcsin\left(\sqrt{\frac{B_0}{B_2}}\right), \tag{1}$$

where B_0 is the magnetic field intensity in the scattering region, and B_1 and B_2 are the magnetic field intensities in the two coronal loop feet, as indicated in the insert of Fig. 2. Taking the magnetic field orientation from loop foot 1 to loop foot 2, the particles leaving the scattering region with pitch-angle $\phi < \alpha_2$ or $\phi > \pi - \alpha_1$ will precipitate.

The equation for the model is a Fokker–Planck equation for the pitch-angle distribution function, where the diffusion tensor and the coefficient of dynamical friction adopt simplified expressions when one assumes that the test particles are fast electrons traveling in a fully ionized plasma with only one kind of positively charged ions (see for example Sivukhin, 1966). All of these simplifying assumptions allow us to derive analytic solutions which show the effects of the asymmetry.

The model solution depends strongly on the diffusion regime. A strong diffusion regime takes place when the change in the pitch-angle in the particle travel through the scattering region is $\Delta\phi \gtrsim \pi/2$. If $t = L/v$ is the required time for a particle of speed v to pass through a scattering region of size L and diffusion coefficient $\mathscr{D}$ (asymmetry in pitch-angle diffusion implies $\mathscr{D} = \mathscr{D}(\phi)$); then, strong diffusion corresponds to

$$\mathscr{D}t \gg \alpha_1^2, \alpha_2^2. \tag{2}$$

In the opposite limit, weak diffusion is when the change in the pitch-angle is small. In this case we have

$$\mathscr{D}t \ll \alpha_1^2, \alpha_2^2. \tag{3}$$

As we will see below, the appropriate limit in our case is the weak diffusion regime.

In the weak diffusion regime the precipitation rates, R_1 and R_2, satisfy

$$\frac{R_1}{R_2} = \frac{\sqrt{\frac{\alpha_1}{\alpha_2}}\exp\left(\frac{\alpha_1-\alpha_2}{\sqrt{t\mathscr{D}}}\right)F(\ell)}{1-\sqrt{\frac{\alpha_1}{\alpha_2}}\exp\left(\frac{\alpha_1-\alpha_2}{\sqrt{t\mathscr{D}}}\right)F(\ell)}, \tag{4}$$

where

$$\ell = \frac{[\mathscr{D}(\phi) - \mathscr{D}(\pi-\phi)]\cos\phi}{[\mathscr{D}(\phi) + \mathscr{D}(\pi-\phi)]|\cos\phi|} \tag{5}$$

is a measure of the asymmetry in the scattering and

Table 1
Parameters derived from microwave spectral fittings: δ corresponds to the electron index, B to the source magnetic field, H and D are the source dimensions (assuming a cylindrical shape), n_e is the number density of the accelerated electrons with energy $E > E_0$, E_0 and E_f are the low and high energy cutoffs, respectively. N_T represents the accelerated electron total number in each source and n the electronic density of the source. The six former parameters are inputs in Ramaty's code, while the two last are outputs.

	δ	B [G]	D [arcsec]	H [10^9 cm]	n_e [10^8 cm^{-3}]	E_0 [keV]	E_f [MeV]	N_T	n [cm^{-3}]
Source 1	3.50	170	10.95	1.9	5.4	17	10	4.78×10^{35}	2.8×10^9
Source 2	2.13	2000	0.17	0.1	5.0	26	10	5.56×10^{30}	3.8×10^{11}

$$F(\ell) = \sqrt{2(1+\ell)}\frac{\sqrt{1+\ell}+\sqrt{1-\ell}}{\sqrt{2}+\sqrt{1+\ell}}. \quad (6)$$

Derivation of Eqs. (4) and (6) can be found in Melrose and White (1981). These results let us compute approximately the different precipitation rates of energetic electrons in a coronal loop.

3.2. Results

We first concentrate in the determination of the diffusion coefficient as function of the velocity for our source parameters. From Trubnikov (1965) and Sivukhin (1966) the pitch-angle diffusion coefficient for Coulomb collisions of fast test particles γ in a fully ionized plasma of particles β is

$$\mathscr{D} = \sum_{\beta} \frac{2\pi q_\gamma^2 q_\beta^2 n_\beta \ln \Lambda_{\gamma\beta}}{m_\gamma^2 v_\gamma^3}, \quad (7)$$

where q_γ and q_β are the electric charges of the particles, n_β is the plasma numerical density, m_γ and v_γ are the mass and velocity of the test particles and $\ln \Lambda_{\gamma\beta}$ is the Coulomb logarithm. We consider fast electrons in a fully ionized plasma of H, then $q_\gamma^2 = q_\beta^2 = e^2$ and m_γ is the electron mass m_e. Then

$$\mathscr{D} = \frac{2\pi e^4 n(\ln \Lambda_{ee} + \ln \Lambda_{ep})}{m_e^2 v^3}. \quad (8)$$

We estimate the possible values of the diffusion coefficient using the plasma parameters derived from the spectral fitting and taking into account that the energy range for the accelerated electrons is 17 keV–10 MeV, meaning that the electron velocities are in the 0.258–0.998 c range. We obtain $0.001 \lesssim \mathscr{D} \lesssim 0.063$. On the other hand, the characteristic travel times of the electrons along the scattering region can be estimated considering, for example, a scattering region size an order of magnitude lower than the coronal loop height (an upper limit to quantify the scattering region size under the localized scattering region hypothesis). Then, depending on the particle energy, $0.007\,\mathrm{s} \lesssim t \lesssim 0.027\,\mathrm{s}$.

We calculate the loss cone values using photospheric observations ($B_1 \approx 2000$ G and $B_2 \approx 450$ G) and the coronal magnetic extrapolation from Paper I ($B_0 \approx 120$ G). The obtained results are, using Eq. (1),

$$\alpha_1 \approx 0.25 \quad \alpha_2 \approx 0.54.$$

The above results let us conclude that the weak diffusion assumption is the suitable limit, since

$$0.002 \lesssim \sqrt{t\mathscr{D}} \lesssim 0.042 \ll \alpha_1, \alpha_2.$$

This result agrees with previous calculations (Melrose and White, 1979).

To evaluate the quotient of the precipitation rates we need to integrate Eq. (4) in the velocity space, taking into account that R_1/R_2 depends on the particle velocity, as can be seen from Eq. (8)

$$\frac{R_1}{R_2}(v) = \frac{\sqrt{\frac{\alpha_1}{\alpha_2}}\exp\left[\frac{(\alpha_1-\alpha_2)v^2 m_e}{\sqrt{2\pi e^4 nL(\ln\Lambda_{ee}+\ln\Lambda_{ep})}}\right]F(\ell)}{1-\sqrt{\frac{\alpha_1}{\alpha_2}}\exp\left[\frac{(\alpha_1-\alpha_2)v^2 m_e}{\sqrt{2\pi e^4 nL(\ln\Lambda_{ee}+\ln\Lambda_{ep})}}\right]F(\ell)}, \quad (9)$$

where L is the diffusion region size and ℓ is considered a parameter (further, we analyse the results for suitable ℓ values). Therefore, the quotient of the total number of precipitated particles in each loop feet is

$$\frac{Q_1}{Q_2} = \frac{\int \frac{R_1}{R_2}(v) N(v) d^3 v}{\int N(v) d^3 v}, \quad (10)$$

where $N(v)$ is the velocity distribution function of the accelerated electrons. From the spectral fit we have an energy distribution function for the fast electron population that follows a power law ($N(E) = KE^{-\delta}$); then, it is convenient to write Eq. (10) in terms of the energy. A simple transformation gives

$$\frac{Q_1}{Q_2} = \frac{\int \frac{R_1}{R_2}(E) E^{-\delta-3}\sqrt{1-\left(\frac{m_e c^2}{E}\right)^2}\,dE}{\int E^{-\delta-3}\sqrt{1-\left(\frac{m_e c^2}{E}\right)^2}\,dE}, \quad (11)$$

with

$$\frac{R_1}{R_2}(E) = \frac{\sqrt{\frac{\alpha_1}{\alpha_2}}\exp\left[\frac{(\alpha_1-\alpha_2)\left(1-m_e^2c^4E^{-2}\right)m_e c^2}{\sqrt{2\pi e^4 nL(\ln\Lambda_{ee}+\ln\Lambda_{ep})}}\right]F(\ell)}{1-\sqrt{\frac{\alpha_1}{\alpha_2}}\exp\left[\frac{(\alpha_1-\alpha_2)\left(1-m_e^2c^4E^{-2}\right)m_e c^2}{\sqrt{2\pi e^4 nL(\ln\Lambda_{ee}+\ln\Lambda_{ep})}}\right]F(\ell)}. \quad (12)$$

All of the required parameters to solve the integral in Eq. (11) are taken from Source 2 parameters (this choice will be justified in Section 4). The lower and upper limits of the integral are taken as the lower (E_0, using the corresponding relativistic value) and upper (E_f) energy cutoffs, respectively. Typical values are used for the Coulomb logarithm ($\ln \Lambda_{ee}$, $\ln \Lambda_{ep} \approx 20$). For the scattering region size (L) a 10% of the loop height value ($H \approx 1.9 \times 10^9$ cm) is used in the calculations; as we already mentioned, this is an upper bound to the scattering region size.

From its definition (see Eq. (5)) the value of ℓ ranges from -1 to 1. A value of $\ell = 0$ corresponds to symmetric scattering (i.e., $\mathscr{D}(\pi-\phi) = \mathscr{D}(\phi)$), while $\ell = 1$ and $\ell = -1$ correspond to limit cases: only scattering of electrons moving parallel or antiparallel to the magnetic field (see Fig. 2). As an example of this extreme case ($\ell = \pm 1$), scattering of electrons by whistlers can be considered (Melrose and White, 1981); for whistlers propagating to the right, only electrons propagating to the left are scattered, because electrons propagating to the right cannot resonate with the whistlers. If the scattering is due to Coulomb interactions, it is expected that this source of asymmetry is unimportant ($\ell \approx 0$); therefore, we restrict our computation to the range $-0.5 < \ell < 0.5$.

The results for the quotient of the total number of precipitated electrons in each coronal feet is shown in Fig. 4 as a function of ℓ. The precipitation in the foot with the larger

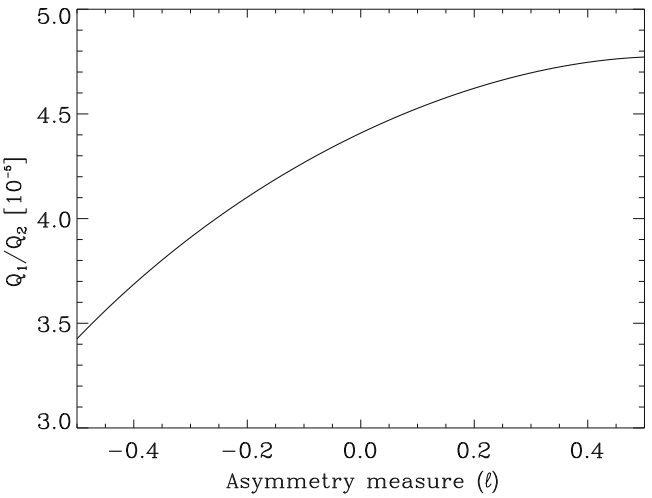

Fig. 4. Precipitation ratio as function of the asymmetry measure value (ℓ).

magnetic field intensity is approximately 5 orders of magnitude less than the one corresponding to the other foot.

Instead of considering the model of Section 3.1, if we only take into account the asymmetry in the field (geometrical asymmetry) the electron precipitation in each feet would not be so different, since the square of the loss cones ratio is $(\alpha_1/\alpha_2)^2 \approx 0.25$. Taking into account this result, we can try to fit the observed spectrum as the superposition of two sources with total electron numbers satisfying $N_{T1}/N_{T2} \approx 0.25$. The low-frequency part of the spectrum is well-constrained; thus, the ranges of the main spectral fit parameters (energy spectral index δ, electron beam density n_e, magnetic field strength B and source size) are restricted. As δ governs the slope of the decaying part of the spectrum, its value is well determined from the observations. The turn-over frequency is mainly determined by the magnetic field strength. The values for the low magnetic field source (referred as Source 2) are then restricted to the ranges:

$$3.4 \leqslant \delta_2 \leqslant 3.6,$$
$$140\ \mathrm{G} \leqslant B_2 \leqslant 190\ \mathrm{G},$$
$$3.5 \times 10^8\ \mathrm{cm}^{-3} \leqslant n_{e2} \leqslant 5.9 \times 10^8\ \mathrm{cm}^{-3},$$
$$2.4 \times 10^{26}\ \mathrm{cm}^3 \leqslant V_2 \leqslant 4.7 \times 10^{26}\ \mathrm{cm}^3,$$

where V_2 stands for the volume. Then, the total number of the accelerated electrons N_{T2} ranges from 3.7×10^{35} to 5.2×10^{35}. This result imposes $0.9 \times 10^{35} \leqslant N_{T1} \leqslant 1.3 \times 10^{35}$ (i.e., we take $N_{T1}/N_{T2} \approx 0.25$). The magnetic field strength B_1 must be large enough to show a turn-over around 200 GHz and $n_{e1} \times V_1 \approx 0.25 \times n_{e2} \times V_2$. We consider a wide range for the parameters:

$$B_1 \gtrsim 2000\ \mathrm{G},$$
$$0.8 \times 10^8\ \mathrm{cm}^{-3} \leqslant n_{e1} \leqslant 6 \times 10^9\ \mathrm{cm}^{-3},$$
$$5 \times 10^{24}\ \mathrm{cm}^3 \leqslant V_1 \leqslant 5 \times 10^{26}\ \mathrm{cm}^3,$$
$$\delta_1 \rightarrow \text{without restrictions.}$$

Here n_{e1} and V_1 were combined to satisfy $0.9 \times 10^{35} \leqslant N_{T1} \leqslant 1.3 \times 10^{35}$. For all possible combinations, we obtain very high flux values, which exceed the observed ones in almost three orders of magnitude at submillimeter wavelengths. This is an expected result because the maximum gyrosynchrotron emission is roughly proportional to N_T and to $B^{\delta+1}$; thus, the flux due to N_{T1} ($N_{T1} \approx 0.25 N_{T2}$) electrons in a B_1 ($B_1 \approx 10 B_2$) magnetic field must be, at least, equal to the emission produced by N_{T2} electrons in a B_2 magnetic field. Therefore, it is not possible to fit the observed spectrum considering two homogeneous sources with total electron numbers of the same order and our spectral model (within small variations) is the only one adequated to explain the observed emission.

4. Discussion and conclusions

Two components or a multicomponent microwave spectrum have been used to explain the observed spectra assuming gyrosynchrotron emission. Analysing the observed temporal evolution Stähli et al. (1990) classified these spectra in two groups: those spectra originated by two separated gyrosynchrotron sources (see for example Gary and Hurford, 1990; Herrmann et al., 1997; Cristiani et al., 2007) and those triggered by a single source or two sources that are strongly coupled (see Huang and Haisheng, 2006).

In this work, we explore the possibility that an unusual spectrum observed in the microwave–submillimeter range can be produced because of the asymmetric rate of precipitation in the loop feet. The explanation for these different precipitation rates is the magnetic field asymmetry derived from a coronal magnetic field extrapolation in Paper I.

In Section 2 the spectral fit is obtained proposing the existence of two homogeneous sources of gyrosynchrotron emission. On the other hand, in Section 3.2, we propose a differential rate of precipitation as an explanation of the observed spectra. These scenarios are not contradictory, as can be inferred in view of the results of Section 3.2. The gyrosynchrotron emission from most of the coronal loop, with magnetic field intensities in the $120\ \mathrm{G} \lesssim B \lesssim 450\ \mathrm{G}$ range, can be associated with Source 2, while the gyrosynchrotron emission in the loop foot with the most intense magnetic field ($B \approx 2000$ G) can be linked to Source 1. Taking into account these results, the magnetic field of Source 2 represents an average or effective magnetic field value all along the coronal loop. The number of the accelerated electrons at Source 1 is approximately 5 orders of magnitude lower than that at Source 2 (see Table 1); this ratio agrees with the quotient of the total precipitation in each coronal feet (Q_1/Q_2). The ambient plasma density differs in 2 orders of magnitude from Source 2 to Source 1; this reinforces the picture of an extended source (Source 2) with a low plasma density (in average) and a concentrated source (Source 1) with high plasma density (with almost chromospheric values).

Other parameter to consider is the electron index for the two proposed sources ($\delta = 3.5$ for Source 2 and $\delta = 2.1$ for Source 1). If these sources could be considered as originating from a single electron population, in principle, we would expect that this population would have the same δ in both sources. Concerning this apparent contradiction, we can argue that the trapping time in a magnetic mirror is proportional to v^{-3}, then, an accelerated electron population hardens (δ takes lower values) and the precipitation of the less energetic particles increases the low energy cutoff ($E_0 = 26$ keV for Source 1, while $E_0 = 17$ keV for Source 2); so, the two proposed sources cannot exist simultaneously. In fact, our observations in microwaves and submillimeter waves are not simultaneous, because they correspond to different radiotelescopes, with different temporal resolution. The flux density at 212 GHz shows a delay of approximately 3 s with respect to the emission at microwaves (see Paper I). To quantify if this time is enough to produce the discussed electron population hardening, a time-dependent model of the evolution of the electron distribution function is necessary, which is out of the scope of this work. Nevertheless, we can estimate trapping times in the weak-diffusion limit (Spitzer, 1956; Trubnikov, 1965; Schmidt, 1979; Benz, 1993; Aschwanden, 1998). For the plasma densities involved in the analysed loop (considering Source 1, which shows the harder electron population) the trapping time of 1 MeV electrons is around 3–4 s, while the trapping time of 100 keV electrons is lower than 0.5 s. The MeV electrons are responsible for the submillimeter emission, while the microwave emission is mainly produced by electrons of hundreds of keVs; then, the trapping time analysis is compatible with the observed time delays between submillimeter and microwave data. Moreover, the analysis reveals that the electron population hardening is relatively fast.

We want to remark that the value of δ for Source 1 is not univocally determined from observations. This value is imposed to prevent values higher than 2000 G for the magnetic field intensity (deduced from photospheric observations). For example, if we take the same value of δ for Source 1 and Source 2, then, the magnetic field intensity needed to fit the submillimeter range of the spectrum is close to 5000 G. On the other hand, simulations taking into account the non-thermal electron distribution evolution in a coronal loop (Fletcher, 1995) show the possibility of the coexistence of two different electron populations in a unique loop, a population associated to the loop top (softer) and another one associated to the feet (harder). The two electron populations originate from an isotropic electron distribution which is injected at the top of the loop. These simulations agree with spatially resolved hard X-ray observations during the impulsive phases of certain compact solar flares (Masuda, 1994; Aschwanden et al., 1997; Metcalf and Alexander, 1999). In synthesis, simulations and observations endorse the scenario of two sources spatially separated with different electron populations, as we have suggested in our analysis; nevertheless, the poor spatial resolution of our data does not permit us to obtain a more direct confirmation.

As the gyrosynchrotron emission depends on the magnetic field strength, as well as the number of the accelerated electrons precipitated per second, high precipitation asymmetry, as the one observed in this event, is susceptible to be detected in radiofrequencies because low number of precipitated electrons in one loop foot is compensated by a high magnetic field intensity. Conversely, hard X-ray emission, which depends on the number of accelerated electrons precipitated per second, cannot show this asymmetric precipitation because the emission in one loop foot is already 5 orders of magnitude lower than the emission in the other one, in the case analysed here. Thus, the limited dynamic range of current hard X-ray detectors prevents the observation of phenomena similar to the one discussed in this paper.

Although this event does not show a rising spectrum in the submillimeter range (212–405 GHz data), the observed enhanced emission at 212 GHz let us classify it as a THz burst, which can be explained exclusively as gyrosynchrotron emission of a source with singular characteristics, unlike the previously observed THz bursts.

As a final remark, we note that the unusual small precipitation ratio was revealed only when the microwave were complemented with the submillimeter observations showing the importance of the latter in bringing new (or yet unobserved) aspects of the flare dynamics.

Acknowledgements

C.G.G.C. acknowledges Ministerio de Ciencia Tecnología e Innovación Productiva, Argentina, for the support through its program RAICES in the frame of which this work was developed. This research was partially supported by the Brazilian agency FAPESP (contract 99/06126-7) and by the Argentinean Grants: UBACyT X127 (UBA) and PIPs 6220 (CONICET). C.H.M., M.G.R. and G.C. are members of the Carrera del Investigador Científico (CONICET). The authors are in debt with A. Magun who released the observations from the Bern patrol telescopes and with T. Lüthi who reduced and gave us the observations of the nulling interferometer at 89.4 GHz. The authors are also grateful to the referees for suggesting improvements to the manuscript.

References

Aschwanden, M.J. Deconvolution of directly precipitating and trap-precipitating electrons in solar flare hard X-rays. I. Method and tests. ApJ 502, 455–467, 1998.

Aschwanden, M.J., Bynum, R.M., Kosugi, T., Hudson, H.S., Schwartz, R.A. Electron trapping times and trap densities in solar flare loops measured with Compton and YOHKOH. Astrophys. J. 487, 936–955, 1997.

Benz, A.O. (Ed.), Plasma Astrophysics: Kinetic Processes in Solar and Stellar Coronae, vol. 184. Astrophysics and Space Science Library, 1993.

Cristiani, G., Giménez de Castro, C.G., Mandrini, C.H., Machado, M.E., Silva, I.D.B.E., Kaufmann, P., Rovira, M.G. A solar burst with a

spectral component observed only above 100 GHz during an M class flare. A&A 492, 215–222, 2008.

Cristiani, G., Martinez, G., Mandrini, C.H., Giménez de Castro, C.G., da Silva, C.W., Rovira, M.G., Kaufmann, P. Spatial characterization of a flare using radio observations and magnetic field topology. Sol. Phys. 240, 271–281, 2007.

da Silva, A., Share, G., Murphy, R., Costa, J., Giménez de Castro, C., Raulin, J.-P., Kaufmann, P. Evidence that synchrotron emission from nonthermal electrons produces the increasing submillimeter spectral component in solar flares. Sol. Phys. 245, 311–326, 2007.

Fletcher, L. On the generation of loop-top impulsive hard X-ray sources. A&A 303, L9–L12, 1995.

Gary, D.E., Hurford, G.J. Multifrequency observations of a solar microwave burst with two-dimensional spatial resolution. ApJ 361, 290–299, 1990.

Herrmann, R., Magun, A., Kaufmann, P., Correia, E., Costa, J.E.R., Machado, M.E., Fishman, G.J. Evidence for highly inhomogeneous mm-wave sources during the impulsive flare of May 9, 1991. A&A 317, 232–243, 1997.

Huang, G., Haisheng, J. Radio, hard X-ray, EUV and optical study of September 9, 2002 solar flare. Astrophys. Space Sci. 301, 65–71, 2006.

Kaufmann, P., Costa, J.E.R., Correia, E., Giménez de Castro, C.G., Raulin, J.-P., Silva, A.V.R. Multiple high energy injections at the origin of solar flares, in: Ramaty, R., Mandzhavidze, N. (Eds.), ASP Conf. Ser. 206: High Energy Solar Physics Workshop – Anticipating Hessi, pp. 318–328, 2000.

Kaufmann, P., Raulin, J.P., de Castro, C.G.G., Levato, H., Gary, D.E., Costa, J.E.R., Marun, A., Pereyra, P., Silva, A.V.R., Correia, E. A new solar burst spectral component emitting only in the terahertz range. ApJL 603, L121–L124, 2004.

Kaufmann, P., Trottet, G., Giménez de Castro, C., Raulin, J., Gary, D., Fernandez, G., Godoy, R., Levato, H., Marun, A., Pereyra, P. Solar burst submillimeter wave emission components associated to microwaves, Uv, X- and γ-rays continuum in time and space, in: American Astronomical Society Meeting Abstracts, vol. 210. American Astronomical Society Meeting Abstracts, pp. 93–93, 2007.

Lüthi, T., Magun, A., Miller, M. First observation of a solar X-class flare in the submillimeter range with KOSMA. A&A 415, 1123–1132, 2004.

Masuda, S. Hard X-ray Sources and the Primary Energy Release Site in Solar Flares. Ph.D. Thesis, Dissertation, Yohkoh HXT Group, NAO, Mitaka, Tokyo, 1994.

Melrose, D.B., White, S.M. Effect of asymmetry on a trap model for solar hard X-ray bursts. Proc. Astron. Soc. Austr. 3, 369–371, 1979.

Melrose, D.B., White, S.M. Precipitation from an asymmetric magnetic flux tube. J. Geophys. Res. 86, 2183–2190, 1981.

Metcalf, T.R., Alexander, D. Coronal trapping of energetic flare particles: Yohkoh/HXT observations. ApJ 522, 1108–1116, 1999.

Schmidt, G. Physics of High Temperature Plasmas, second ed. Academic Press, Inc?, New York, 1979.

Sivukhin, D.V. Coulomb collisions in a fully ionized plasma. Rev. Plasma Phys. 4, 93–241, 1966.

Spitzer, L. Physics of Fully Ionized Gases. Interscience Publishers, New York, 1956.

Stähli, M., Gary, D.E., Hurford, G.J. The secondary spectral component of solar microwave bursts. Sol. Phys. 125, 343–357, 1990.

Trubnikov, B.A. Particle interactions in a fully ionized plasma. Rev. Plasma Phys. 1, 105–200, 1965.